


Article

High-Temperature Mechanical Properties and Microstructure of Ultrathin 3003mod Aluminum Alloy Fins

Wenhui Zheng¹, Chengyuan Ni^{1,*}, Chengdong Xia^{1,2,*}, Shaohui Deng¹, Xiaoying Jiang^{1,2} and Wei Xu¹¹ College of Mechanical Engineering, Quzhou University, Quzhou 324000, China² Zhejiang Bulaoshen Civil Air Protection Equipment Co., Ltd., Quzhou 324022, China

* Correspondence: nichengyuan1@126.com (C.N.); xcd309@163.com (C.X.);

Tel.: +86-135-6704-8900 (C.N.); +86-158-6147-9982 (C.X.)

Abstract: The effects of Si, Fe and Zr elements on the high temperature properties and microstructure of ultrathin 3003mod aluminum alloy fins were studied by means of high-temperature tensile tests, sagging tests and microstructure analyses. The results show that the alloying of Si, Fe, and Zr elements formed a large amount of nano-scale α -Al(Mn,Fe) Si and Al_3Zr particles, and significantly reduced the number of micro-scale coarse $\text{Al}_6(\text{Mn,Fe})$ particles in the 3003mod aluminum alloy, exhibiting 5 to 10 MPa higher strength and better sagging resistance than 3003 aluminum alloy at the same temperature. The variations in properties such as high-temperature mechanical properties, sagging resistance and elongation below 400 °C were ascribed to the high-stability nanoparticles effectively preventing recovery and grain boundary migration, as well as reducing the nucleation cores of recrystallization. The nanoparticles in 3003mod aluminum alloy were coarsened significantly at 500 °C, and the grains were completely recrystallized and coarsened, resulted in a significant decrease in strength, sagging resistance and elongation compared with these at 400 °C.

Keywords: 3003 aluminum alloy; alloying; high temperature strength; sagging distance; recrystallization



Citation: Zheng, W.; Ni, C.; Xia, C.; Deng, S.; Jiang, X.; Xu, W. High-Temperature Mechanical Properties and Microstructure of Ultrathin 3003mod Aluminum Alloy Fins. *Metals* **2024**, *14*, 142. <https://doi.org/10.3390/met14020142>

Academic Editor: Amogelang Bolokang

Received: 19 December 2023

Revised: 19 January 2024

Accepted: 22 January 2024

Published: 24 January 2024



Copyright: © 2024 by the authors. Licensee MDPI, Basel, Switzerland. This article is an open access article distributed under the terms and conditions of the Creative Commons Attribution (CC BY) license (<https://creativecommons.org/licenses/by/4.0/>).

1. Introduction

As a main component of a heat exchanger, fins dissipate heat from tube or plate materials into the air by increasing the surface area of the heat exchanger. Fin materials usually include a steel strip, a copper strip, and an aluminum strip. Due to its characteristics of light weight, suitable strength, good corrosion resistance, thermal conductivity, brazing and processing formability, $3 \times \times \times$ series aluminum alloy has become the main fin material for heat exchangers [1–4].

With the increasingly urgent trend of seeking out lightweight aluminum heat exchangers, it is required that aluminum alloys become thinner and thinner. At present, the thickness of the aluminum alloy foil used in commercial fins is usually 0.07 mm, and the lightweight demands require the fin thickness to reach 0.05 mm or even thinner. After the aluminum alloy fin is thinned, the thickness of the supporting material decreases accordingly, resulting in a decrease in the load that the fin can withstand, and it can easily sag and delaminate during brazing at around 600 °C [5–9]. Therefore, improving the high-temperature properties and reducing the thickness of fins has always been the goal of this type material. Alloying is an effective way to improve the high temperature strength of $3 \times \times \times$ series alloys for heat exchangers. The addition of Zr alloy to $3 \times \times \times$ series aluminum alloy could generate Al_3Zr nanoparticles coherent with the matrix, which effectively inhibit the occurrence of recrystallization during high-temperature brazing, prevent the softening of the alloy used in heat exchangers, and improve its own strength [10,11]. When trace amounts of Si and Zr elements are added together with $3 \times \times \times$ aluminum alloy, the post-brazed grain structure was refined with increasing Si contents, and Zr addition led to larger post-brazed grain structures [12]. Minor additions of Cd, Cr and Si content also

considerably improved mechanical strength after heating to between 350 and 600 °C due to the finer size, higher density, lower diffusivity and more homogeneous distribution of dispersoids [13]. Zinc is a common alloying element used in aluminum alloys to improve their strength, but it reduces the conductivity, ductility, weldability and fracture toughness by segregating along grain boundaries, enhancing the solute dragging effect and forming zinc-containing phases [14–17]. However, due to the small difference in atomic radius between Al and Zn, and the limited solid solubility of Zn in aluminum up to 32.8%, adding 1–2 wt.% Zn to aluminum makes little contribution to the mechanical properties of the alloy [18]. The main reason for adding Zn to pure aluminum is attributed to its significant impact on corrosion performance, which could dramatically reduce the potential of aluminum alloy and significantly improve the stress corrosion cracking (SCC) resistance of the alloys [19,20], such that Zn-containing aluminum alloys are generally used as a sacrifice material for heat exchangers to protect the tube or plate material with higher corrosion potential. Due to the significantly lower strength of ultrathin $3 \times \times \times$ aluminum alloy at high temperatures compared to room temperature, and the very low load required for fracturing in high-temperature tensile tests (<200 N), it is extremely difficult to test high-temperature mechanical properties. Therefore, there are currently few reports on the high-temperature properties of ultrathin $3 \times \times \times$ aluminum alloy fins.

In this paper, a 3003 aluminum alloy was modified by alloying of Si, Fe, Zr and Zn elements, and a non-contact, low-load high-temperature tensile test and sagging test were used to study the high-temperature properties of the ultrathin aluminum alloy fins, explore the high-temperature properties and microstructure evolution of ultrathin aluminum alloy materials at different tensile temperatures, and analyze the action mechanism of alloying elements. This is expected to provide theoretical guidance for the development of ultrathin aluminum alloy fins with good high-temperature properties.

2. Materials and Methods

2.1. Material and Preparation

Based on the chemical composition of 3003 aluminum alloy, a modified 3003 (named 3003mod) aluminum alloy was designed by adding a minor Zr element, increasing the content of Si and reducing the content of Fe. The 3003 and 3003mod aluminum alloys' chemical compositions in this study are shown in Table 1. In addition, 1.5 wt.% Zn was added to the 3003mod aluminum alloy to reduce the corrosion potential of the fins, so that the alloy could be used as a sacrifice material to protect the tube or plate material of the heat exchanger. Pure aluminum, Al-Mn10 master alloy, pure silicon, Al-Fe80 master alloy, Al-Zr10 master alloy, and Al-Ti15 master alloy were melted and refined at 700–760 °C in accordance with the designed composition, and then semi-continuously cast into ingots with a thickness of 450 mm at Yinbang Clad Material Co., Ltd., Wuxi, China. After surface milling and preheating at 480 °C for 2 h, the ingots were hot-rolled to 6 mm in thickness, and then cold-rolled to strips with a thickness of 0.115 mm. After annealing at 350 °C for 2 h and a final cold-rolling, ultrathin aluminum alloy fins with a thickness of 0.07 mm and a state of H14 were prepared.

Table 1. 3003 and 3003mod aluminum alloys' chemical composition (wt.%).

Alloy	Si	Fe	Mn	Zn	Ti	Zr	Al
3003	0.15	0.5	1.5	0.05	0.025	/	Balance
3003mod	0.55	0.2	1.5	1.5	0.025	0.15	Balance

2.2. Test Methods

2.2.1. Tensile Test

A Zwick-010 high-temperature tensile machine (ZwickRoell, Ulm, Germany) equipped with a laser extensometer and resistance heating furnace was used for the test, and a manual fine-toothed jig was installed in the sealed furnace. The temperature limit of the

test environment was 600 °C, and the maximum load of the tensile sensor was 500 N, with a loading accuracy of 1% of the actual load. Waste aluminum foil was used to wrap around the gripping end of the tensile sample (3–5 layers) to prevent the clamping die from damaging the clamping end of the specimen to be stretched. The high-temperature tensile tests were carried out in accordance with ISO 6892-2 [21]. Loading began after the heating temperature reached the set temperature and was held for 5 min. The preload used in the high-temperature tensile test was 5 MPa. During the tensile test, the stretching speed from the elastic stage to the upper yield point stage was 0.75 mm/min, and the stretching speed from the upper yield point to fracture was 1.125 mm/min. The precision of stretching temperature was ± 3 °C from room temperature to 500 °C. Three samples were tested at each temperature, and we took the average of the test values. The sample size of the high-temperature tensile test is shown in Figure 1.

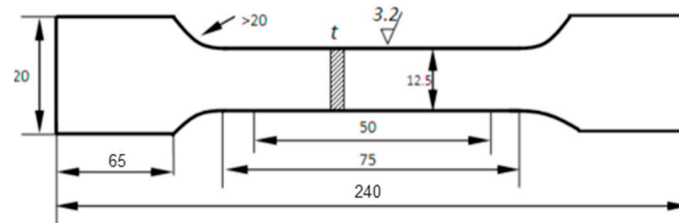


Figure 1. Sample size of tensile test.

2.2.2. Sagging Test

A sagging test was applied to characterize the sagging behavior of ultrathin aluminum alloy fins. The test rig is shown in Figure 2. The fins were cut into samples of 100 mm in the rolling direction and 15 mm in the reverse direction. One end of the sample was fixed, and the length of the free end was 50 mm, as shown in Figure 2a. The sagging test rig with the sample was heated to various temperatures (up to a brazing temperature of 600 °C) with a heating rate of 25 °C/min and removed from the furnace after holding for 5 min; then, the sagging distance was calculated by subtracting the height after brazing from the height before brazing, as shown in Figure 2b. The sagging distance at each temperature represents the sagging resistance of cold-rolled aluminum fins.

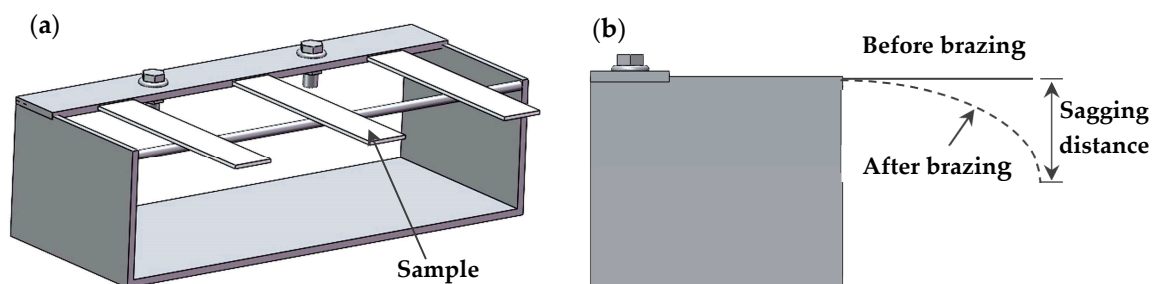


Figure 2. Schematic of sagging test rig (a) and sagging distance (b).

2.2.3. Microstructure Analysis

The cast samples and finished product samples parallel to the rolling direction were cut and then cold-set with resin. After mechanical grinding and polishing, the metallographic samples were prepared via electrochemical polishing with coating solutions of 5 mL HF, 10 mL HNO₃ and 85 mL H₂O, and then were observed and analyzed using a Zeiss Axio Imager A2 optical microscope. The microstructure and chemical composition of the selected area were analyzed using a Zeiss-Sigma thermal field emission scanning electron microscope (SEM, CARL ZEISS, Oberkochen, Germany) with an energy dispersive spectrometer (EDS, Oxford Instruments, Abingdon, UK) under an accelerating voltage of 10–20 kV. Transmission electron microscope (TEM) samples were prepared by twin-jet

polishing using a solution of 10% perchloric acid in methanol, and analyzed on a JEOL-2100 transmission electron microscope (JEOL Ltd., Akishima, Japan) operating at 200 kV.

3. Results

3.1. High-Temperature Mechanical Properties of Ultrathin Aluminum Alloy Fins

The tensile mechanical properties of 3003 and 3003mod aluminum alloys at different temperatures are shown in Figure 3. As can be observed from the figure, with the increase in temperature, both the tensile strength and yield strength of 3003 and 3003mod aluminum alloy displayed decreasing trends, and the amount of this decrease was similar. The tensile strength and yield strength of 3003mod alloy at room temperature were 187 MPa and 178 MPa, respectively, which are 4.5% and 1.7% higher than those of 3003 alloy. The tensile strength and yield strength of 3003mod alloy at 100 °C were 3.2% and 2.6% higher than those of the 3003 alloy, respectively. Similarly, the tensile strength and yield strength of 3003mod alloy were 15.7% and 12.6% higher than those of the 3003 alloy at 300 °C, respectively, while they were 22.2% and 27.3% higher than those of 3003 alloy at 400 °C, and 42.9% and 50% higher at 500 °C, respectively. The rates of reduction rate in the tensile strength and yield strength of the 3003mod alloy were 62.9%, 44.1%, 39.4% and 65.4%, 48.1% and 35.7%, respectively, while rates of the reduction in the 3003 alloy were 66.9%, 47.1%, 48.1% and 68.4%, 54.2% and 45.5%, respectively. The above results indicate that the 3003mod alloy had a higher high-temperature strength at the same test temperature, and the strength of 3003mod alloy was less affected by temperature than that of the 3003 alloy. In terms of elongation, the 3003 and 3003mod aluminum alloys first elongated with the increase in test temperature, and then decreased sharply after reaching a peak at 400 °C. The elongation of the 3003mod alloy was greater than that of the 3003 alloy at each temperature.

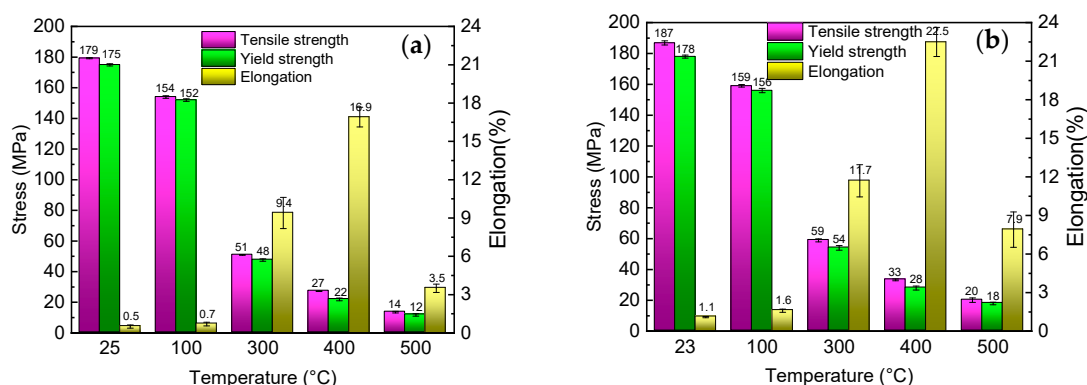


Figure 3. Tensile mechanical properties of 3003 (a) and 3003mod (b) aluminum alloys at different temperatures.

3.2. Sagging Properties of Ultrathin Aluminum Alloy Fins

Figure 4 shows the sagging distances of 3003 and 3003mod aluminum alloys after being held at various temperatures for 5 min. As can be seen from the figure, when the temperature increased from room temperature to 100 °C, there was no obvious sagging in the 3003 and 3003mod alloys. When it continued to rise to 300 °C, both alloys showed slight sagging, but the sagging value was very small. As the temperature increased to 400 °C, the 3003 and 3003mod aluminum alloys exhibited sharp sagging, with average sagging distances of about 14 mm and 12 mm. After holding at 500 °C for 5 min, the average sagging distances of the 3003 and 3003mod aluminum alloys increased to 16.5 mm and 14 mm, respectively. The sagging test results indicate that 3003mod alloy had better sagging resistance properties than 3003 alloy.

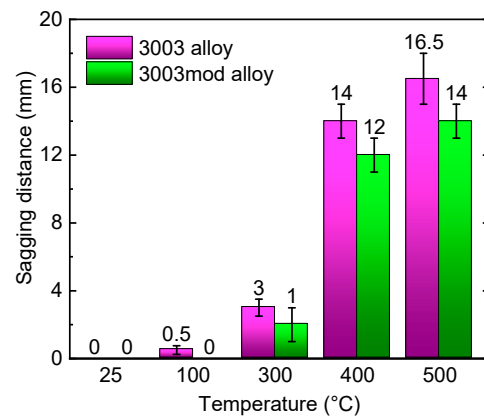


Figure 4. Sagging properties of 3003 and 3003mod aluminum alloys at different temperatures.

3.3. Microstructure of Cast 3003 and 3003mod Aluminum Alloys

Figure 5 shows the cast microstructure and EDS analysis results of the 3003 and 3003mod aluminum alloys. As shown in the figure, there are a large number of grain boundaries distributed in a network and composed of eutectic structures in the 3003 aluminum alloy. The eutectic structure inside the 3003mod ingot is significantly reduced, and most grain boundaries are discontinuously distributed in a tridentate shape. The scanning electron microscope backscatter electron image clearly displays a dark matrix and bright white coarse particles, among which the size and shape of the coarse particles in the 3003 aluminum alloy are similar to those in the 3003mod aluminum alloy, but the density is much higher than that in the 3003mod aluminum alloy. The bright white coarse particles in the EDS results for the 3003 aluminum alloy show that the coarse particles mainly contain four elements: Al, Fe, Mn, and Si. In addition to the matrix, the element with the highest mass fraction is Fe, followed by Mn. The coarse particles in the 3003mod aluminum alloy are also in the Al–Fe–Mn–Si phase, but the element with the highest content besides Al is Mn. It is worth noting that the Al content in the coarse phase of 3003 and 3003mod aluminum alloys is within the range of 73–75 wt.%. This result indicates that the adjustment of Si, Fe, and Zr elements causes a change in the proportions of Fe and Mn in the coarse particles, but hardly changes the Al content. On the other hand, it significantly reduces the number of coarse particles in the as-cast alloy.

3.4. Microstructure of Ultrathin Aluminum Alloy Fins

3.4.1. Metallographic Microstructure at Various Temperatures

Figure 6 exhibits the metallographic microstructures of 3003 and 3003mod aluminum alloys with insulation for 5 min at different stretching temperatures. As shown in the figure, no significant changes occur in the grain sizes of 3003 and 3003mod aluminum alloys at room temperature, with both maintaining a relatively large aspect ratio. The number of grains in the thickness direction of 3003 alloy foil was about three to five, and it was significantly elongated along the rolling direction, with an average grain length greater than 800 μm , while the 3003mod alloy had two to three grains in the thickness direction, and the average length of the elongated grains in the rolling direction was greater than 1000 μm . Partial recrystallization began to occur in the thickness direction of the 3003 alloy foil at 300 $^{\circ}\text{C}$, as shown by the arrow in Figure 6b, while there was no obvious change in grains in the 3003mod alloy. When the temperature was increased to 400 $^{\circ}\text{C}$, a significant recrystallization phenomenon occurred in the 3003 alloy, with a sharp decrease in the aspect ratio. However, only partial recrystallization occurred in the 3003mod alloy, and the grains still maintained a large aspect ratio, as shown by the arrow in Figure 6g. When further increasing the temperature to 500 $^{\circ}\text{C}$, the aspect ratio of 3003 aluminum alloy further decreased, and the grains tended to be equiaxed, while the grains of the 3003mod aluminum alloy coarsened to one to two grains across the entire thickness.

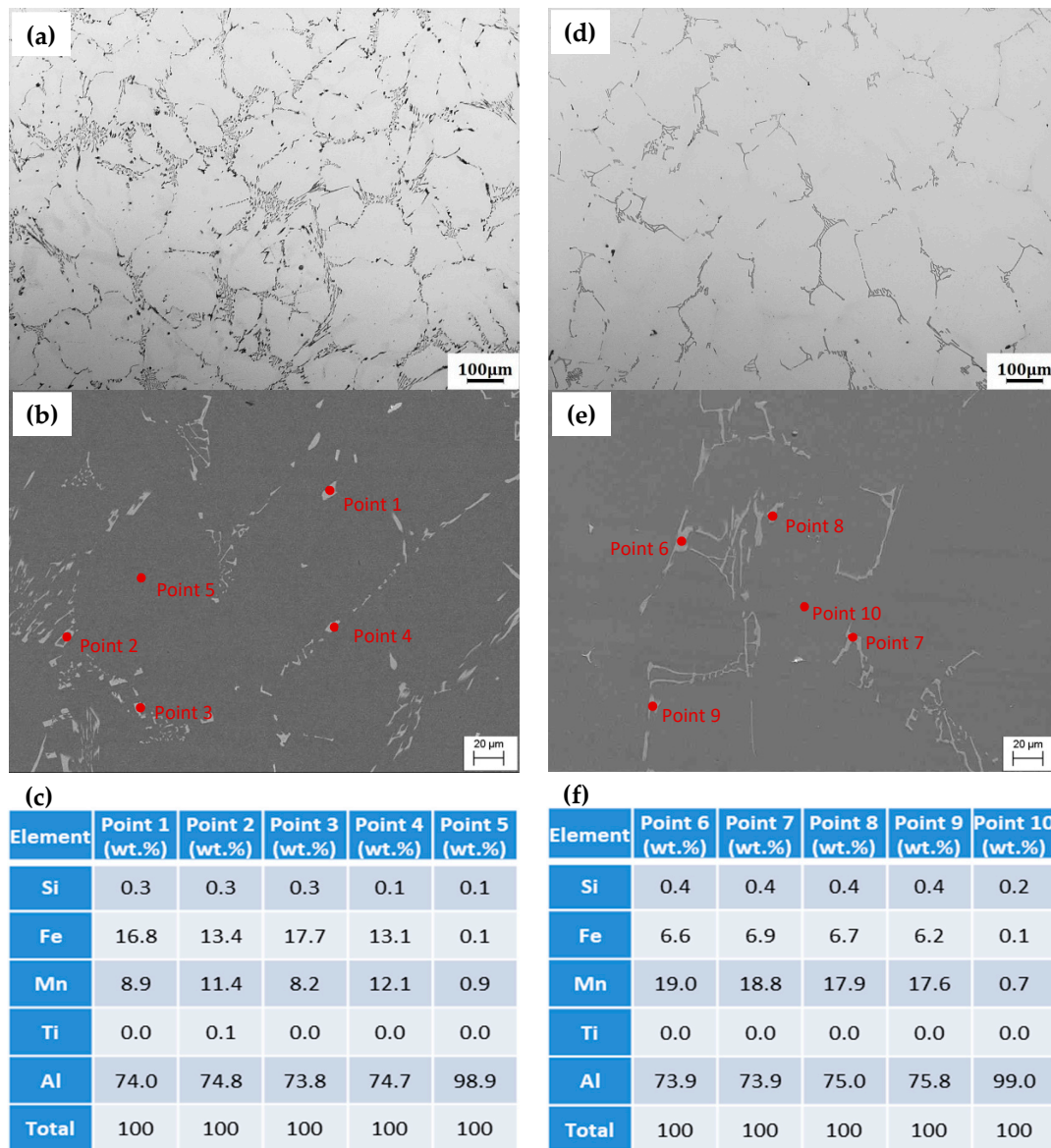


Figure 5. Microstructure and EDS analysis results of cast 3003 and 3003mod aluminum alloys. (a–c) Metallographic photograph, SEM image and EDS of 3003 aluminum alloy. (d–f) Metallographic photograph, SEM image and EDS of 3003mod aluminum alloy.

3.4.2. SEM Microstructure at Different Temperatures

Figure 7 displays the SEM images of 3003 and 3003mod aluminum alloys at room temperature. It can be seen that the eutectic structure of the cast 3003 and 3003mod aluminum alloys was fractured by the large deformation of hot-rolling and cold-rolling. Therefore, a large number of micro-scale coarse particles were dispersed inside the material, and a large amount of dispersed nano-scale particles could also be observed in the 3003mod alloy. A locally enlarged image of the 3003mod aluminum alloy is shown in Figure 7c. These dispersed particles were nearly spherical or elliptical, and about 20–100 nm in size. The corresponding results of the EDS analysis of the nano-scale particles are shown in Figure 7d. The results show that these nanoparticles mainly contained elements such as Al, Mn, Si, Fe, and Ti, and the total contents of Mn and Fe were much lower than those of micron-sized coarse particles. Comparing the EDS of coarse particles and nanoparticles in 3003 and 3003mod aluminum alloys, it can be inferred that the excessive content of Fe in the aluminum alloy tended to form micro-scale coarse particles, while elements such

as Si and Ti tended to form dispersed nanoparticles. Therefore, adding the Zr element, reducing the Fe content, and increasing the Si content are all beneficial to the formation of dispersed nanoparticles.

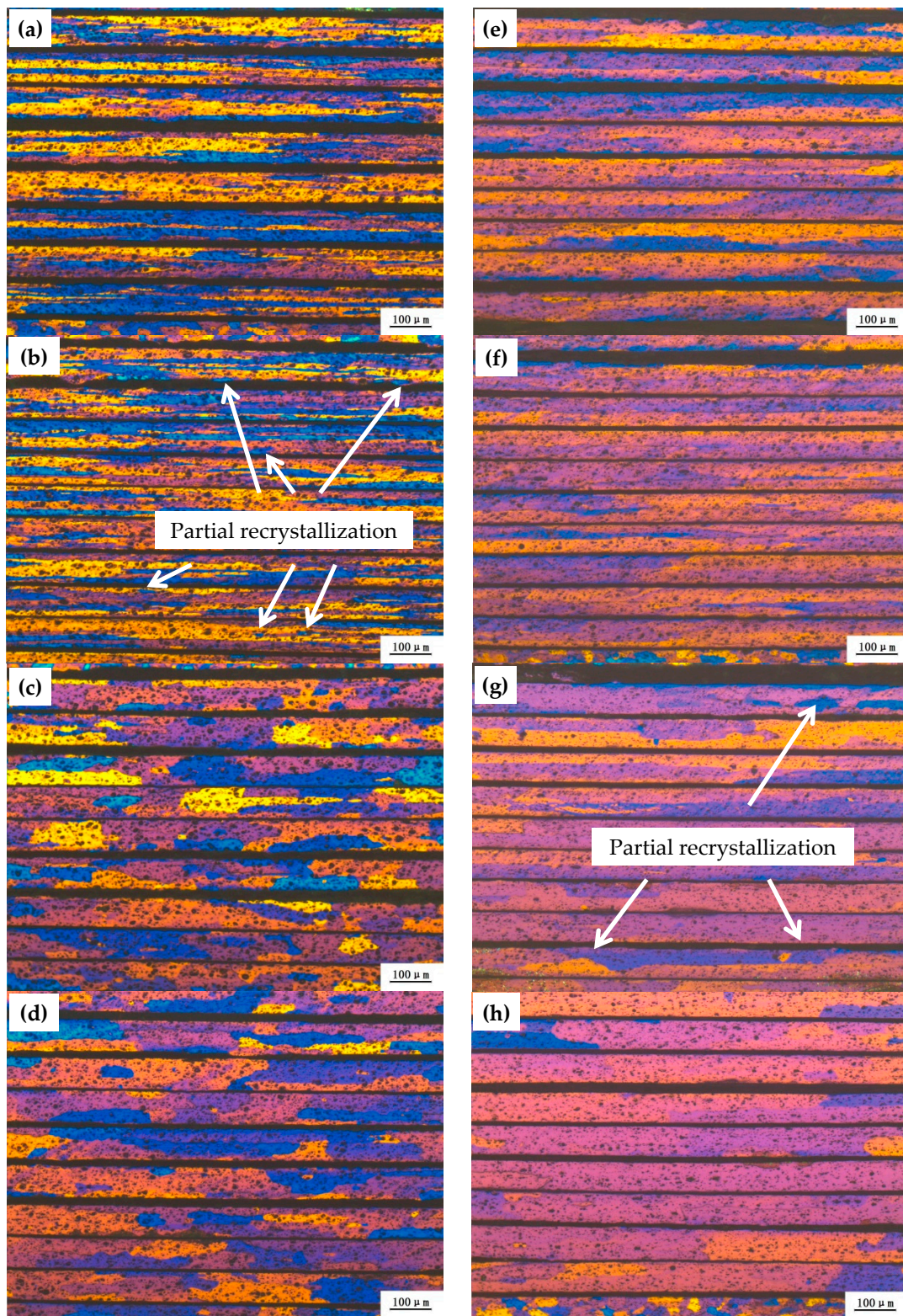


Figure 6. Metallographic microstructure of 3003 and 3003mod aluminum alloys at different temperatures (a) 3003—room temperature; (b) 3003—300 °C; (c) 3003—400 °C; (d) 3003—500 °C; (e) 3003mod room temperature; (f) 3003mod—300 °C; (g) 3003mod—400 °C; (h) 3003mod—500 °C.

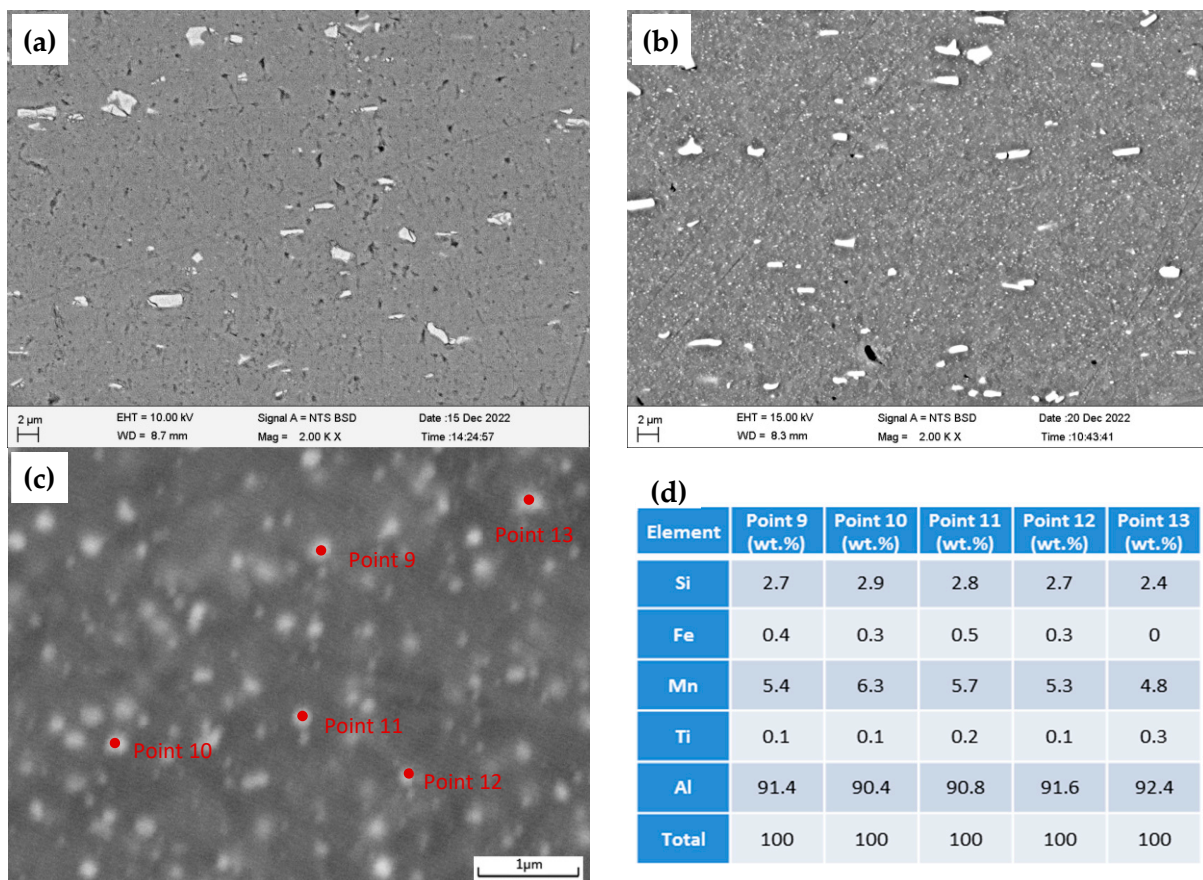


Figure 7. SEM images and EDS analysis results of 3003 and 3003mod aluminum alloy fin at room temperature: (a) 3003 aluminum alloy; (b) 3003mod aluminum alloy; (c) locally enlarged 3003mod aluminum alloy; (d) EDS results in (c).

Figure 8 shows SEM images and the size distribution of nanoparticles of the 3003mod alloy at different temperatures for 5 min. It can be seen from the SEM images that there were a large number of nanoparticles in 3003mod at different temperatures, most of which were nearly circular or elliptical. Statistical analyses of the size distribution are shown in Figure 8b,d,f,g, and the area fractions of nanoparticles at different temperatures can be calculated using the software of ImageJ (Java 1.8.0_322). The results show that the average size of nanoparticles in the 3003mod alloy at room temperature was approximately 95 nm, with an area fraction of approximately 8.5%, while the average size of nanoparticles was 103 nm with an area fraction of approximately 7.8% at 300 °C. When the holding temperature was increased to 400 °C, the particles coarsened, and the average particle size was about 110 nm, while the area fraction was about 7.0%. When further increasing the holding temperature to 500 °C, the average particle size reached 135 nm, and the area fraction was about 4.9%. This result indicates that the nanoparticles in 3003mod have good thermal stability and show minimal changes below 400 °C, while when the holding temperature increased to 500 °C, the nanoparticles began to significantly coarsen, and the particle density gradually decreased. On the other hand, the solid solubilities of elements such as Mn, Fe and Si in the matrix also increased with the temperatures, leading to a decrease in the area fraction of nanoparticles.

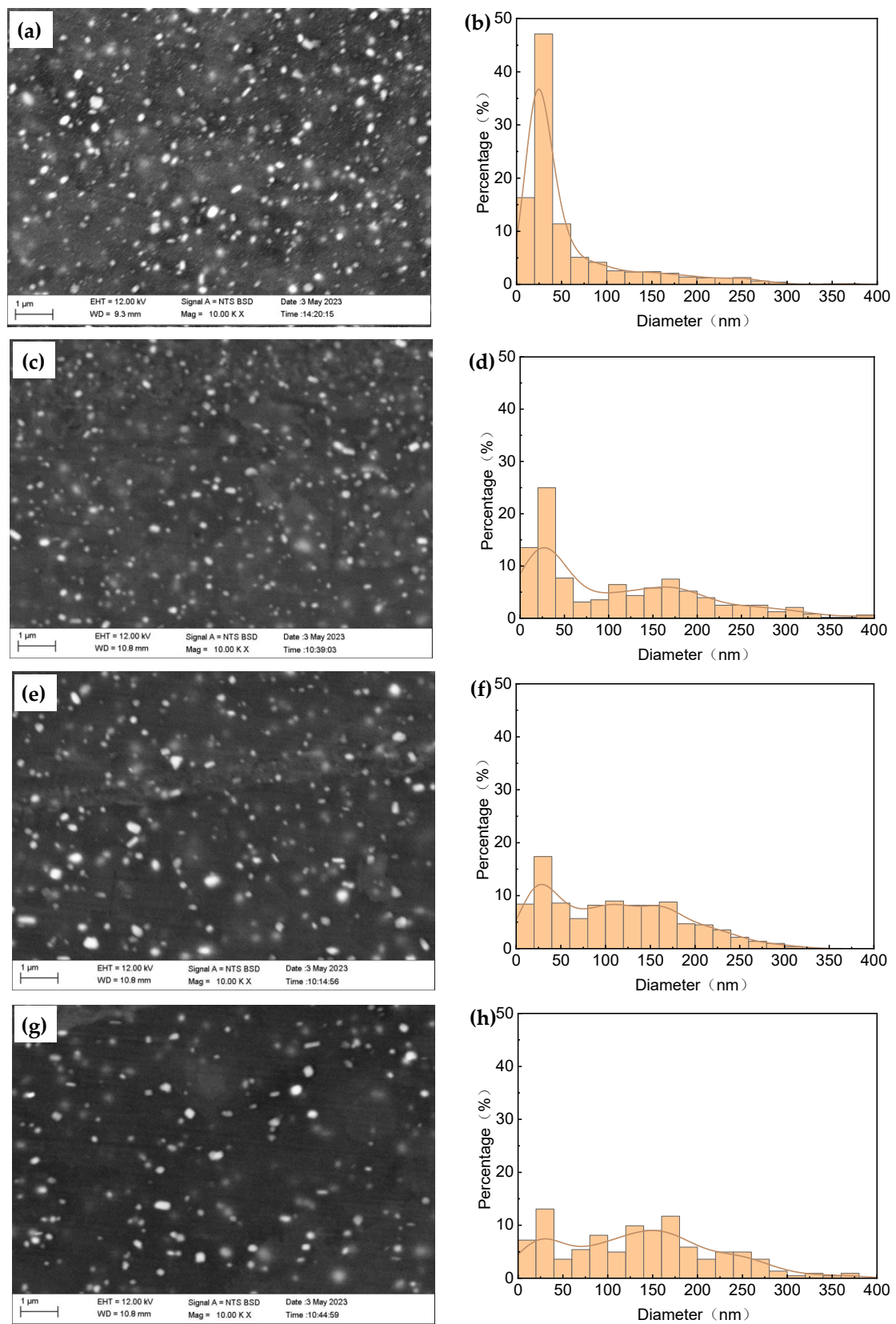


Figure 8. SEM images and nanoparticles' size distribution of 3003mod aluminum alloy at different temperatures: (a,b) Room temperature; (c,d) 300 °C; (e,f) 400 °C; (g,h) 500 °C.

3.4.3. TEM Microstructure at Different Temperatures

Figure 9 displays TEM images of the 3003mod aluminum alloy held for 5 min at different temperatures. High-density dislocation entanglement can be observed in the recrystallization-annealed and 40% cold-rolled 3003mod aluminum alloy. A recovery phenomenon occurred inside the alloy, and the internal microstructure contained a large number of dislocation cells after being held at 300 °C and 400 °C. During holding at 300 °C, a certain density of dislocations inside the cell could still be seen, while after being insulated at 400 °C, the dislocation cell structure grew, and the dislocation density inside the cell decreased significantly, with a small amount of fine recrystallized grains appearing. Further increases in the insulation temperature to 500 °C, with no dislocation cells in the entire field of view, and coarse nanoparticles with a size greater than 100 nm could be observed. This result shows that the grains of the 3003mod aluminum alloy finished recrystallization, and grew and coarsened at this temperature.

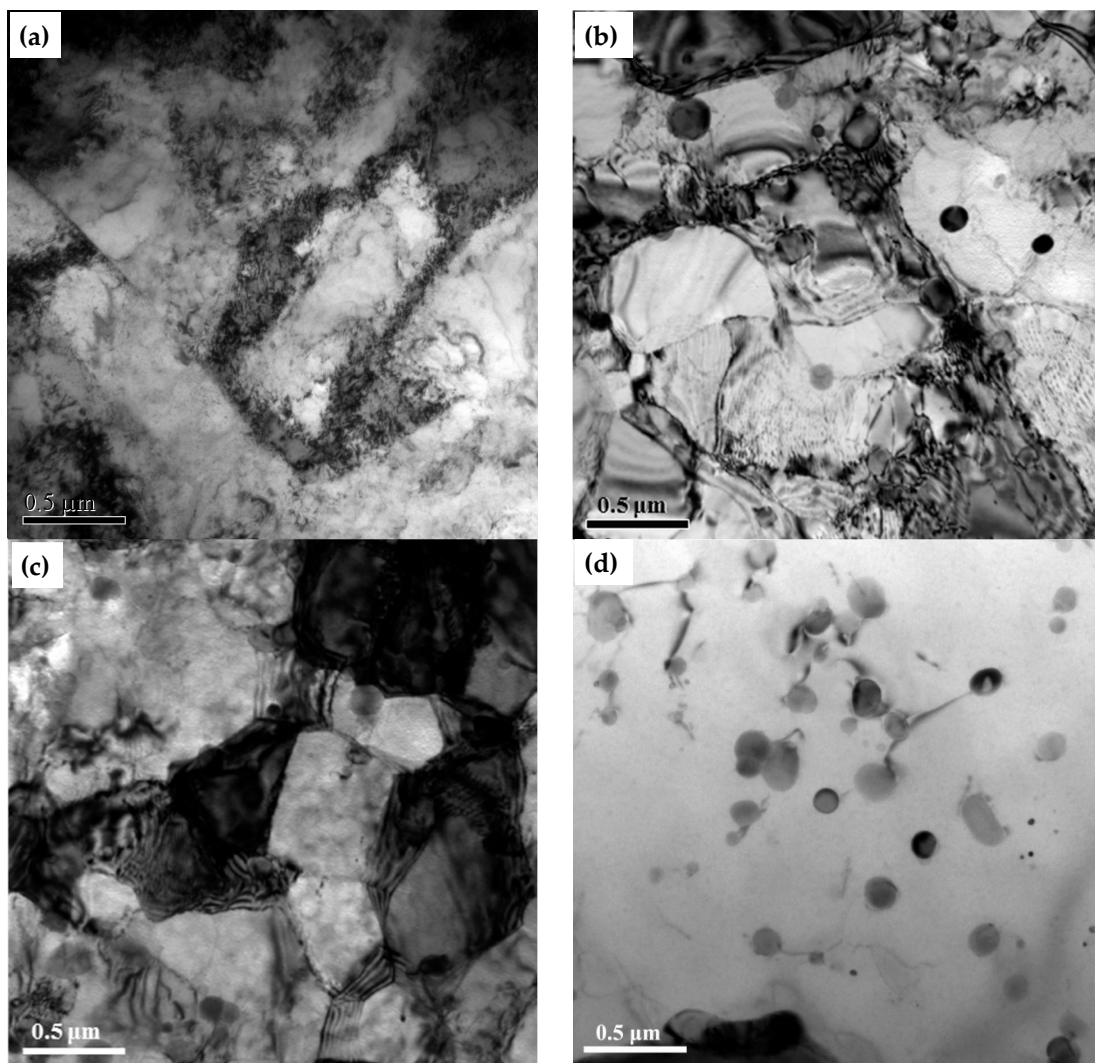


Figure 9. TEM images of 3003mod aluminum alloy at different temperatures. (a) Room temperature; (b) 300 °C; (c) 400 °C; (d) 500 °C.

4. Discussion

4.1. The Influence of Alloying on the Mechanical Properties of Aluminum Alloy Fins

In the manufacturing of heat exchangers, it is necessary that the fin material maintain a certain mechanical strength at a maximum brazing temperature of about 600 °C in order to prevent sagging and deformation, or even cracking during brazing [6,7]. At such

high temperatures, aluminum alloys will inevitably undergo phenomena such as recovery, recrystallization, grain growth, second phase particle growth, particle redissolution, intergranular erosion, and slip deformation at grain boundaries, leading to a sharp decline in their mechanical properties [6–9,22–24]. On the other hand, grain boundaries show viscosity at high temperatures, which greatly reduces the resistance to deformation [25]. The more grain boundaries there are, the lower the high-temperature yield strength of the material. Therefore, in order to achieve good high-temperature performance in ultrathin fin materials, it is suggested that the fins show a thickness of one to two grains at high temperatures, and the grain's length can be over 1 mm [5–8].

In order to improve the mechanical properties of aluminum alloy fin materials at high temperatures, researchers have carried out a lot of work. On the one hand, good mechanical and sagging resistance properties could be obtained through the optimization of the processing technology. Broer [4] revealed that the mechanical properties resulting from homogenization at lower temperatures could show an increase of approximately 40% compared to the reference homogenization at 550 °C. Kang [9] studied the effects of annealing and deformation on the sagging resistance of 4433/3003/6111/3003 clad sheet, and the results show that low-temperature annealing and a small amount of coarse recrystallized grains could suppress the erosion of Si, resulting in better sagging resistance and strength. On the other hand, alloying to produce dispersed and high-temperature-resistant fine particles is also an effective method to improve high-temperature strengths [11–13,26]. The Al_3Zr or $(\text{Al,Si})_3\text{Zr}$ precipitates that are formed by the addition of Si and Zr played a major role in retarding recrystallization during brazing [11]. Cd, Cr and increased Si content can also considerably improve the mechanical strength after heating to between 350 and 600 °C due to the finer size, higher density, lower diffusivity and more homogeneous distribution of dispersoids [13].

This study designed and prepared a 3003mod aluminum alloy by adding the minor Zr element, increasing the Si content and reducing the Fe content, resulting in a significant reduction in the number of coarse particles, and changes in the contents of Mn and Fe in the coarse particles, while the aluminum content remained basically unchanged compared with the 3003 alloy, as shown in Figures 5 and 6. According to the EDS analysis results and references [27,28], it can be inferred that the dispersed nano-scale particles in the 3003mod aluminum alloy were $\alpha\text{-Al}(\text{Mn,Fe})\text{Si}$ and Al_3Zr , while the micro-scale coarse particles were in the $\text{Al}_6(\text{Mn,Fe})$ phases. Both $\alpha\text{-Al}(\text{Mn,Fe})\text{Si}$ and Al_3Zr exhibit good heat resistance, according to the results in Figure 8. These nano-scale particles could significantly inhibit the occurrence of recrystallization nucleation by exerting strong pinning effects on the movements of dislocations and grain boundaries during high-temperature recovery and recrystallization [26,29–31]. The coarse $\text{Al}_6(\text{Mn,Fe})$ phases in the alloy also have very high thermal stability, and could serve as recrystallization cores for nucleation due to their large size [12,28,32]. In this study, a large number of nano-scale particles were formed and micro-scale coarse particles were apparently reduced in the 3003mod aluminum alloy compared with the 3003 aluminum alloy. The nano-scale particles led to dispersion strengthening, and retarded the recovery process and growth of recrystallized grains, while the nucleation sites of recrystallization were reduced due to the reduction in coarse particles during the high-temperature tensile or sagging tests, as shown in Figures 3, 6 and 9. These results are ascribed to the coarser grain size and higher recrystallization temperature of the 3003mod aluminum alloy at high temperatures. Finally, the tensile strength and yield strength of the 3003mod aluminum alloy were both 5 to 10 MPa higher than those of the 3003 aluminum alloy at the same temperature, while the sagging values were lower than those of 3003 aluminum alloy at the same temperature (in the range of room temperature to 500 °C), as shown in Figures 3 and 4. Improving the mechanical properties could correspondingly reduce the thickness of the material under the same conditions, which has strong practical significance regarding the pursuit of lightweight heat exchangers. With the increase in test temperature, the coarsening and redissolution of nanoparticles led to a significant decrease in the area fraction of nanoparticles, resulting in a significant weakening or even disap-

pearance of the dispersion strengthening and retardation effect, leading to the complete recrystallization and coarseness of grains at high temperatures, and a sharp decrease in mechanical properties at high temperatures.

4.2. The Influence of Alloying on the Elongation of Aluminum Alloy Fins

Since the grain boundary strength is higher than the intragrain strength at low temperatures, the cold plastic deformation mechanism of polycrystalline materials mainly comprises intragrain slip and twinning. At the same time, a small amount of grain boundary sliding and migration can coordinate the plastic deformation of adjacent grains [25]. Therefore, a small grain size could significantly improve the elongation of the material. The main plastic deformation modes are grain boundary sliding and migration during high-temperature deformation due to the lower strength of the grain boundaries compared to the internal grains [25]. Therefore, the smaller the grain size, the less favorable its plastic deformation is.

In this study, the amount of micro-scale coarse $Al_6(Mn,Fe)$ was significantly reduced by adjusting the alloying elements. Although the contribution of micro-sized particles to the strength of materials can be almost negligible, due to the significant differences in strength and plasticity toughness between coarse particles and the matrix, it is easy for the matrix to be cut and form a crack source during tensile deformation, which greatly affects the plasticity of the material. The reduction in the number of coarse particles results in the greater elongation of the 3003mod aluminum alloy at all test temperatures compared to the 3003 aluminum alloy, as shown in Figure 3.

For ultrathin fins, on the one hand, due to the limited number of grains in the thickness direction, the coordinated plastic deformation of grain boundaries at room temperature is considerably reduced. On the other hand, 40% final cold-rolling deformation results in a high dislocation density, so the elongation at room temperature under this condition is only 0.7~1.1%, as shown in Figures 6 and 9. When the tensile test temperature was raised to 300 °C, the grains and particles in the 3003 and 3003mod aluminum alloy fins did not exhibit obvious changes. However, there was evident recovery inside the grains, and the dislocation density decreased dramatically, as shown in Figure 9b, resulting in an increase in elongation. When continuing to increase the temperature of the tensile test to 400 °C, the 3003 aluminum alloy underwent significant recrystallization, while the nucleation of recrystallization only occurred locally in the 3003mod alloy, with almost no dislocations observed inside the grains, resulting in a significant increase in elongation. When the tensile test temperature reached 500 °C, the 3003 alloy generally showed complete recrystallization, while a few areas remained in the 3003mod alloy that showed a large aspect ratio with a large grain structure. The average grain size here was significantly decreased compared to 300 °C, and the coarsening of nanoparticles inhibited any increase in the number of grains. Under a tensile load at 500 °C, the resistance of grain boundaries to deformation was greatly reduced, and the nanoparticles were considerably coarsened. Both grain boundaries and coarsened nanoparticles became the source of cracks. Therefore, the degree of tensile elongation in 3003mod aluminum alloy fins at 500 °C was much lower than that at 400 °C. The variations in tensile elongation in 3003 and 3003mod alloys under high temperature test conditions were the result of the synergistic effects of grain size and second phase particles in the two alloys.

5. Conclusions

- (1) The tensile strength and yield strength of the 3003mod aluminum alloy fins modified with Si, Fe, Zr and Zn elements were both 5 to 10 MPa higher than those of the 3003 aluminum alloy at the same temperature, while the sagging values were lower than those seen for the 3003 aluminum alloy at the same temperature in the range of room temperature to 500 °C. This result is of great significance to further reducing the thickness of the fins and thus achieving lightweight heat exchangers;

- (2) Many α -Al (Mn,Fe) Si and Al_3Zr nano-scale particles were formed, and the number of coarse $\text{Al}_6(\text{Mn,Fe})$ particles was significantly reduced, in the 3003mod aluminum alloy by changing the proportion and distribution of Mn, Fe and Si in the particles compared to the 3003 aluminum alloy;
- (3) High-stability nanoparticles effectively prevented recovery and grain boundary migration during the tensile process at temperatures below 400 °C, while the reduction in the number of coarse particles decreased the number of recrystallization nucleation cores, which synergistically led to stronger high-temperature mechanical properties, better sagging resistance, and the greater elongation of the 3003mod aluminum alloy;
- (4) The nanoparticles in the 3003mod aluminum alloy were coarsened significantly at 500 °C, and the grains were completely recrystallized and coarsened, resulting in a significant decrease in strength, sagging resistance and elongation compared with these properties at 400 °C.

Author Contributions: Conceptualization, C.N. and C.X.; methodology, W.Z., S.D., C.N. and C.X.; investigation, W.Z., S.D., X.J. and W.X.; data curation, W.Z., S.D., X.J. and W.X.; writing—original draft preparation, W.Z., S.D. and X.J.; writing—review and editing, C.N., C.X., S.D. and X.J.; visualization, S.D., X.J. and W.X.; supervision, C.N. and C.X.; funding acquisition, C.N. and C.X. All authors have read and agreed to the published version of the manuscript.

Funding: This research was funded by the National College Students' Innovation and Entrepreneurship Training Program (No. 202211488008), Zhejiang College Students' Innovation and Entrepreneurship Training Program (No. 2022R435A004), the Joint Funds of the Zhejiang Provincial Natural Science Foundation of China (No. LZ Y23E010001 and LZ Y22E010002), Quzhou Science and Technology Bureau (No. 2021K26, 2023K210).

Data Availability Statement: Data are contained within the article.

Acknowledgments: The authors thank Jianping Yu who comes from Zhejiang Bulaoshen Civil Air Protection Equipment Co., Ltd. for the preparation and photographing of metallographic samples for this research, and we also thank Yan An from Yinbang Clad Material Co., Ltd. for his support in material acquisition and high-temperature tensile testing.

Conflicts of Interest: Author Chengdong Xia was employed by the company Zhejiang Bulaoshen Civil Air Protection Equipment Co., Ltd. The remaining authors declare that the research was conducted in the absence of any commercial or financial relationships that could be construed as a potential conflict of interest.

References

1. Jin, H. Development of an aluminum brazing sheet product with barrier layer for high-performance automotive heat exchangers. *Metall. Mater. Trans. A* **2021**, *52*, 1409–1426. [[CrossRef](#)]
2. Moema, J.S.; Siyasiya, C.W.; Morudu, V.K.; Buthelezi, T. The effect of soaking time on mechanical properties of roll-bonded AA3003 and AA4045 used for heat exchangers. *Metals* **2023**, *13*, 1636. [[CrossRef](#)]
3. Zhang, J.X.; Sun, H.Y.; Du, P.; Liu, W.C. Effect of processing method on the recrystallization behavior of cold-rolled AA3003 aluminum alloy. *J. Mater. Eng. Perform.* **2020**, *29*, 4286–4294. [[CrossRef](#)]
4. Broer, J.; Mallow, S.; Oldenburg, K.; Milkereit, B.; Kessler, O. The influence of homogenisation parameters on the microstructure and hardness of AlMnFeMgSi(Zr) wrought alloys. *Metals* **2023**, *13*, 1706. [[CrossRef](#)]
5. Qin, J.N.; Kang, S.B.; Cho, J.H. Sagging mechanisms in the brazing of aluminum heat exchangers. *Scr. Mater.* **2013**, *68*, 941–944. [[CrossRef](#)]
6. Liu, C.W.; Xue, X.L.; Chen, X.; Li, L.; Xia, C.D.; Zhong, Z.J.; Zhou, D.J. Effect of microstructural evolution on sagging behavior of cold-rolled aluminum foil during the brazing thermal cycle. *J. Mater. Eng. Perform.* **2017**, *26*, 5563–5570. [[CrossRef](#)]
7. Tang, C.L.; Xu, Q.P.; Guo, X.F.; Chen, X.; Liu, C.W.; Li, L.; Zhou, D.J. Sagging mechanisms of three-layer aluminum clad foils used in the heat exchanger in the brazing process. *J. Mater. Eng. Perform.* **2018**, *27*, 4846–4854. [[CrossRef](#)]
8. Li, H.; Lu, G.X.; Xu, C.; Guan, S.K. Microstructural evolution and sagging behavior of cold-rolled Al-1.3Mn-1.5Zn-xZr core sheet for brazing. *J. Alloys Compd.* **2022**, *891*, 161927. [[CrossRef](#)]
9. Kang, M.L.; Zhou, L.; Deng, Y.L.; Lei, J.Q. Effects of annealing and deformation on sagging resistance of a hot-rolled, four-layered Al alloy clad sheet. *Adv. Mater. Sci. Eng.* **2021**, *2021*, 6625548. [[CrossRef](#)]
10. Vlach, M.; Stulikova, I.; Smola, B.; Piesova, J.; Cisarova, H.; Danis, S.; Plasek, J.; Gemma, R.; Tanprayoon, D.; Neubert, V. Effect of cold rolling on precipitation processes in Al-Mn-Sc-Zr alloy. *Mater. Sci. Eng. A* **2012**, *548*, 27–32. [[CrossRef](#)]

11. Pan, S.W.; Qian, F.; Li, C.N.; Wang, Z.D.; Li, Y.J. Synergistic strengthening by nano-sized α -Al(Mn,Fe)Si and Al₃Zr dispersoids in a heat-resistant Al-Mn-Fe-Si-Zr alloy. *Mater. Sci. Eng. A* **2021**, *819*, 141460. [[CrossRef](#)]
12. Shimosaka, D.; Ueno, M. Effects of Si and Zr addition on strength and recrystallization behavior of Al-Mn alloy fin stocks for automotive heat exchanger. *MATEC Web Conf.* **2020**, *326*, 05006. [[CrossRef](#)]
13. Qian, F.; Jin, S.B.; Wan, D.; Li, W.Z.; Cheng, X.W.; Sha, G.; Li, Y.J. Synergistic effects of Cd, Si and Cr additions on precipitation strengthening and thermal stability of dispersoids in AA3003 alloy. *Mater. Sci. Eng. A* **2022**, *832*, 142422. [[CrossRef](#)]
14. Zhu, Z.; Jiang, X.; Wei, G.; Fang, X.; Zhong, Z.; Song, K.; Han, J.; Jiang, Z. Influence of Zn content on microstructures, mechanical properties and stress corrosion behavior of AA5083 aluminum alloy. *Acta Metall. Sin.* **2020**, *33*, 1369–1378. [[CrossRef](#)]
15. Zhang, A.; Li, Y. Effect of alloying elements on thermal conductivity of aluminum. *J. Mater. Res.* **2023**, *38*, 2049–2058. [[CrossRef](#)]
16. Jung, S.S.; Hwang, S.B.; Kim, B.J.; Park, Y.H.; Lee, Y.C. Effect of Zn additions on the mechanical properties of high strength Al-Si-Mg-Cu alloys. In *Light Metals 2020*; Tomsett, A., Ed.; The Minerals, Metals & Materials Series; Springer: Cham, Switzerland, 2020. [[CrossRef](#)]
17. Shen, G.; Chen, X.; Yan, J.; Fan, L.; Yang, Z.; Zhang, J.; Guan, R. A review of progress in the study of Al-Mg-Zn(-Cu) wrought alloys. *Metals* **2023**, *13*, 345. [[CrossRef](#)]
18. Davis, J.R. *Aluminum and Aluminum Alloys*, ASM Specialty Handbook; ASM International: Geauga, OH, USA, 1993; pp. 8–695.
19. Meijers, S.D. Corrosion of Aluminum Brazing Sheet. Ph.D. Thesis, Technische Universiteit Delft, Delft, The Netherlands, 2002.
20. Li, Q.; Li, M.; Lu, G.; Guan, S.; Zhang, E.; Xu, C. Effect of trace elements on the crystallization temperature interval and properties of 5xxx series aluminum alloys. *Metals* **2020**, *10*, 483. [[CrossRef](#)]
21. ISO 6892-2:2018; Metallic Materials Tensile Testing. Part 2: Method of Test at Elevated Temperature. ISO: Geneva, Switzerland, 2018. Available online: <https://www.iso.org/standard/72571.html> (accessed on 15 June 2022).
22. Xia, C.D.; Deng, S.H.; Ni, C.Y.; Ji, Y.Y.; Zheng, W.H.; Luo, J.Q.; Xu, W.; Li, W.D.; Pang, Y. Study on laminar structure and process on high strength brazed aluminum alloy for heat exchangers. *Vacuum* **2023**, *215*, 112303. [[CrossRef](#)]
23. Lee, S.H.; Yoon, J.S.; Kim, M.S.; Jung, D. Effects of cold rolling parameters on sagging behavior for three layer Al-Si/Al-Mn(Zn)/Al-Si brazing sheets. *Met. Mater. Int.* **2002**, *8*, 227–232. [[CrossRef](#)]
24. Yoon, J.S.; Lee, S.H.; Kim, M.S. Sagging resistance of cold rolled aluminum 4343/3N03/4343 clad sheet. *J. Mater. Sci. Lett.* **2001**, *20*, 229–232. [[CrossRef](#)]
25. Zheng, Z.Q. *Fundamentals of Materials Science*, 2nd ed.; Central South University Press: Changsha, China, 2005; pp. 328–385.
26. Qian, F.; Jin, S.B.; Sha, G.; Li, Y.J. Enhanced dispersoid precipitation and dispersion strengthening in an Al alloy by microalloying with Cd. *Acta Mater.* **2018**, *157*, 114–125. [[CrossRef](#)]
27. Li, Y.J.; Muggenrud, A.M.F.; Olsen, A.; Furu, T. Precipitation of partially coherent α -Al(Mn,Fe)Si dispersoids and their strengthening effect in AA 3003 alloy. *Acta Mater.* **2012**, *60*, 1004–1014. [[CrossRef](#)]
28. Li, Y.J.; Arnberg, L. Evolution of eutectic intermetallic particles in DC-cast AA3003 alloy during heating and homogenization. *Mater. Sci. Eng. A* **2003**, *347*, 130–135. [[CrossRef](#)]
29. Hansen, V.; Gjonnes, J.; Andersson, B. Quasicrystals as part of the precipitation sequence in an industrially cast aluminium alloy. *J. Mater. Sci. Lett.* **1989**, *8*, 823–826. [[CrossRef](#)]
30. Riddle, Y.W.; Hallem, H.; Ryum, N. Highly recrystallization resistant Al-Mn-Mg alloys using Sc and Zr. *Mater. Sci. Forum* **2002**, *396–402*, 563–568. [[CrossRef](#)]
31. Li, Y.J.; Arnberg, L. Precipitation of dispersoids in DC-cast 3003 alloy. *Mater. Sci. Forum* **2002**, *396–402*, 875–880. [[CrossRef](#)]
32. Karlík, M.; Mánik, T.; Slámová, M.; Lauschmann, H. Effect of Si and Fe on the Recrystallization Response of Al-Mn Alloys with Zr Addition. *Acta Phys. Pol. A* **2012**, *122*, 469–474. [[CrossRef](#)]

Disclaimer/Publisher’s Note: The statements, opinions and data contained in all publications are solely those of the individual author(s) and contributor(s) and not of MDPI and/or the editor(s). MDPI and/or the editor(s) disclaim responsibility for any injury to people or property resulting from any ideas, methods, instructions or products referred to in the content.